energy&fuels

Article

Cite This: Energy Fuels 2019, 33, 4611−4620

pubs.acs.org/EF

Experimental and Kinetic Modeling Studies of Methyl 2-Furoate Pyrolysis at Atmospheric Pressure

Beibei Yan,[†,∥] Jinglan Wang,[†] Qinghui Meng,[§] Zhanjun Cheng,[*,†,∥] Lixia Wei,[*,‡] Yan Zhang,[§] Chuangchuang Cao,[§] Jiuzhong Yang,[§] and Guanyi Chen[†,∥]

[†]School of Environmental Science and Engineering, Tianjin University, Tianjin 300072, P. R. China

[‡]College of Mechanical Engineering, Guangxi University, Nanning, Guangxi 530004, P. R. China

[§]National Synchrotron Radiation Laboratory, University of Science and Technology of China, Hefei, Anhui 230029, P. R. China

[∥]Tianjin Key Lab of Biomass/Wastes Utilization/ Key Laboratory of Biomass-Derived Gas and Oil for Chinese Petrochemical Industry, Tianjin 300072, P. R. China

Supporting Information

ABSTRACT: Methyl 2-furoate (FAME2) pyrolysis was studied experimentally on a flow reactor in the temperature range of 879-1107 K and at the pressure of 760 Torr using synchrotron vacuum ultraviolet photoionization mass spectrometry. Several important intermediates were identified and measured, including the major pyrolysis products (methane, carbon monoxide, acetylene, formaldehyde, carbon dioxide, ketene, and vinyl acetylene) and even isomers of pyrolysis products (propyne, allene, 1,3-butadiene, 1-butyne, fulvene, and benzene). Unimolecular decomposition reactions in the pyrolysis of FAME2 were also studied theoretically at the CBS-QB3 level using the Gaussian procedure. Based on the calculated potential energy surface, a new kinetic model was developed and validated against our pyrolysis experiments. The rate of production and sensitivity analysis revealed that the decomposition reactions of FAME2 are mainly controlled by the unimolecular decomposition reactions, substitution reactions, H-abstraction reactions, and H-addition reactions in FAME2 pyrolysis. The dominant decomposition reaction is the direct release of CH_3 from FAME2, which has about 42% contribution to the fuel consumption.

1. INTRODUCTION

Energy consumption, uneven distribution of oil reserves, increases of global energy demands, and environmental issues together drive research efforts to the development of renewable energy resources.[1] Oxygenated hydrocarbon fuels derived from biomass, with their renewability, near neutral CO_2 emission, and suitable physical and chemical properties, have attracted considerable attention, as replacements of or additives to conventional hydrocarbon fuels in internal combustion engines.[1−4] Long-chain fatty acid methyl esters, as the dominant components of biodiesel, have attracted intensive research studies.[5−11] However, these researches mainly focused on methyl formate (CH_3OCHO),[5] dimethyl carbonate ($CH_3OCOOCH_3$, DMC),[6] methyl propionate ($CH_3CH_2COOCH_3$, MP),[7] methyl butanoate ($CH_3CH_2CH_2COOCH_3$, MB),[8,12] methyl crotonate ($CH_3CH{=}CHCOOCH_3$, MC),[9,12,13] and methyl decanoate.[11,14] Biodiesel, as the first-generation biofuel, produced from vegetable oils by transesterification or cracking, compromises with food supply.[1,3] The second-generation liquid biofuels are generally produced from agricultural lignocellulosic biomass and even non-edible biomass by biological or thermochemical processes. Furan, 2-methylfuran (MF), and especially 2,5-dimethylfuran (DMF) have received intensive attention because of their suitable physical and chemical properties.[1,15−18]

Recently, a new method had been proposed by combining the raw materials of 2-furoic acid (FA2), CO_2, and methanol (CH_3OH) to produce dimethyl furan-2,5-dicarboxylate.[19] Dimethyl furan-2,5-dicarboxylate incorporates FA2, CO_2 sequestrated from the atmosphere, and CH_3OH manufactured from the synthesis gas that comes from natural gas, coal, or biomass, and hence, it is a promising renewable and even carbon negative biofuel. However, before the practical adoption of this fuel, its combustion mechanism should be carefully investigated. Similar to the studies of MF and DMF, methyl 2-furoate (FAME2) is a good starting model compound for the combustion studies of dimethyl furan-2,5-dicarboxylate, with only one methoxycarbonyl group (−C(O)OCH_3, CH_3OCO in this work) in its structure. In this work, the experimental and kinetic modeling studies of FAME2 pyrolysis were investigated.

No results on the pyrolysis of FAME2 have been reported until now. Because the furyl and ester groups in FAME2 are analogous to those in furan derivatives and short-chain fatty acid methyl esters, respectively, the unimolecular decomposition and H-abstraction reactions in the pyrolysis of FAME2 should be similar to those in the pyrolysis of furan, MF, and DMF and CH_3OCHO, DMC, MP, and MC.

There are extensive experimental investigations on the combustion of furan derivatives (furan,[16,20] MF,[21−23] and DMF[24−27]) and short-chain fatty acid methyl esters

Received: February 3, 2019
Revised: April 19, 2019
Published: April 22, 2019

DOI: 10.1021/acs.energyfuels.9b00367
Energy Fuels 2019, 33, 4611−4620

(CH_3OCHO,[5] DMC,[6] MP,[7,28] MB,[9,29] and MC[9,12]) in the past decades, including the speciation in pyrolysis,[7,20,22,24,26] oxidation,[9] and flames,[17,18,23] as well as the measurements of ignition delay times[25−27,30] and laminar burning velocities.[23] Grela et al.[31] determined the decomposition rates of furan, MF, and DMF in a heated flow reactor and analyzed the pyrolysis products using gas chromatography−mass spectrometry at T = 1050−1270 K and p = 1.3 × 10^{-3} Pa. Lifshitz et al.[32−34] studied the three furanic fuels at T = 1050−1460 K and p = 2−3 atm using a shock tube. Mole fraction profiles of the final products were measured using gas chromatography. Recently, Liu et al.,[16] Togbé et al.,[17] and Tran et al.[18] reported the combustion chemistries and flame structures of furan series biofuels using molecular-beam mass spectrometry and gas chromatography. A detailed combustion model of these fuels, based on the model of Tian et al.[35] and Sirjean et al.,[36] was proposed and validated against their low-pressure premixed laminar flames. Cheng et al.[20,22,24] investigated the pyrolysis of furan, MF, and DMF at various pressures in a flow reactor using synchrotron vacuum ultraviolet photoionization mass spectrometry (SVUV-PIMS) and updated the combustion model of Somers et al.[21] As to the investigations on the combustion of fatty acid methyl esters, Gaïl et al.[9,29] studied the oxidation of MB and MC over a wide range of conditions in a jet-stirred reactor with gas chromatography to compare the reactivities of a saturated and an unsaturated ester and developed detailed kinetic models for the combustion of MB and MC. Zhao et al.[7] studied MP pyrolysis in a laminar flow reactor at p = 30 Torr and T = 1000−1500 K, reported the measurements of free radicals and intermediate products, and developed and validated a detailed kinetic model of MP pyrolysis based on their experimental results and theoretical calculations. Recently, Ning et al.[28] studied MP pyrolysis in a shock tube at T = 1292−1551 K and p = 1.6 atm and calculated the direct C−O/C−C bond fissions and molecular reaction channels by using high-level ab initio calculations and Rice−Ramsperger−Kassel−Marcus master equation theory. The improved mechanism could accurately predict the early formation of CO and CO_2 over the entire temperature range. Sun et al.[6] studied flow reactor pyrolysis at p = 40, 200, and 1040 mbar and low-pressure laminar premixed DMC flames with equivalence ratios of 1.0 and 1.5. Their detailed kinetic model developed from theoretical calculations and estimations well reproduced the mole fraction profiles of the detected products and intermediates. The rate of production (ROP) analysis showed that CO_2 was produced directly from the carbonate and ester moieties in DMC rather than the oxidation of CO. Zhai et al.[12] studied the flow reactor pyrolysis of MB and MC at p = 30, 150, and 760 Torr using gas chromatography−mass spectrometry. The results showed that the C═C double bond in MC might strengthen the tendency of initial polycyclic aromatic hydrocarbons (PAHs) and soot precursor formation relative to MB.

In this work, FAME2 pyrolysis was studied in a flow reactor at 760 Torr using SVUV-PIMS to detect the pyrolysis products and measure their mole fraction profiles as a function of temperature, especially important intermediates such as furfural (f2cho, $C_5H_4O_2$), MF, and FA2. The mole fraction profiles of FAME2 pyrolysis species were first reported in the present work. The potential energy surface (PES) for the unimolecular decomposition reactions of FAME2 was characterized using quantum chemical methods at the CBS-QB3 level. A new kinetic model was developed and validated against the new pyrolysis data of FAME2. The decomposition reaction pathways of FAME2 were analyzed based on the present model.

2. EXPERIMENTAL METHODS

The experiments were carried out at the National Synchrotron Radiation Laboratory in Hefei, China. In general, the pyrolysis apparatus consisted of a pyrolysis chamber with a heating furnace, a differentially pumped chamber with a molecular-beam sampling system, and a photoionization chamber combined with a home-made reflectron time-of-flight mass spectrometer, as shown in Figure 1a.

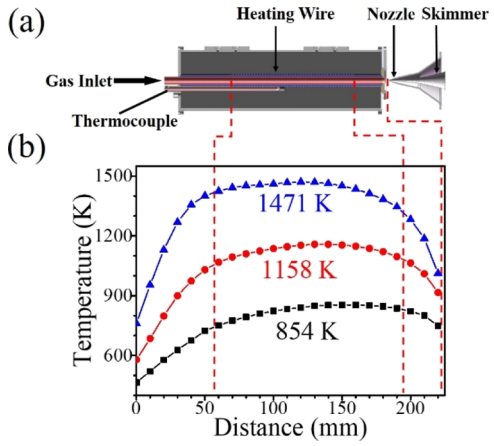

Figure 1. (a) Schematic diagram of the pyrolysis apparatus with a molecular-beam sampling system. (b) Axial temperature profiles of the flow tube measured in this work.

The fuel was fed into the α-alumina flow tube of 7.0 mm inner diameter × 224 mm length and heated by the heating furnace in the pyrolysis chamber. The pyrolysis species were sampled by a quartz nozzle to form a molecular beam in the differentially pumped chamber. Then the molecular beam passed through a nickel skimmer and shot into the photoionization chamber, where the pyrolysis species were ionized by the synchrotron vacuum ultraviolet radiation. The ions were detected and analyzed by the mass spectrometer. For the SVUV-PIMS experiments, the detailed description can be found elsewhere.[37,38]

During the experiments, the total inlet flow rate of FAME2/Ar gaseous mixture (1% of FAME2 by volume) was fixed at 1.000 standard liter per minute. The flow rate of FAME2 was controlled by a liquid chromatography pump (FL2200, Zhejiang Fuli Analytical Instruments Co., Ltd., China) at room temperature and that of Ar was controlled by a mass flow controller (MKS, USA). FAME2 (boiling point 454 K at p = 760 Torr) was vaporized and mixed with Ar in a vaporizer with a temperature of 484 K to ensure efficient vaporization of the sample. FAME2 with a purity of 99% was purchased from Meryer (Shanghai) Chemical Technology Co., Ltd., and Ar with a purity of 99.999% was purchased from Nanjing Special Gases Factory Ltd., China.

Detailed methods of temperature measurements along the axis of the reactor had been introduced in recent studies,[38−41] thus only a brief introduction is provided herein. A tungsten−rhenium thermocouple was mounted near the middle region of the heating wire to monitor the outside temperature (T_{out}) of the flow tube. Before and after each experiment, a platinum−rhodium thermocouple was put inside the flow tube to measure the temperature profiles along the axis of the flow tube. The uncertainty of temperature measurement is within ±30 K. In the present work, each temperature profile along the flow tube is named by the maximum value of the temperature profile (T_{max}), as shown in Figure 1b. Detailed temperature profiles are provided in the Supporting Information. The residence times in this experiment are calculated to be 1.29 ×

DOI: 10.1021/acs.energyfuels.9b00367
Energy Fuels 2019, 33, 4611−4620

Table 1. FAME2 Submechanism[a]

no.	reactions	A	n	E_a	ref
R1	FAME2 = FAO2J + CH_3	8.70×10^{27}	−3.51	7.93×10^{4}	[b]
R2	FAME2 = f2cjo + CH_3O	1.17×10^{77}	−17.79	1.30×10^{5}	[c]
R3	FAME2 = f2j + CH_3OCO	2.07×10^{20}	−1.04	1.15×10^{5}	[d]
R4	FAME2 = f2cho + CH_2O	1.00×10^{12}	0.00	6.05×10^{4}	[e]
R5	FAME2 = MF + CO_2	1.50×10^{12}	0.00	5.98×10^{4}	[f]
R6	FAME2 = f2och3 + CO	6.94×10^{4}	2.62	6.44×10^{4}	[g]
R7	FAME2 = p23de5o1ooch3-t	4.93×10^{11}	0.66	6.87×10^{4}	[g]
R8	FAME2 = p34de2o1ooch3-t	4.93×10^{11}	0.66	6.87×10^{4}	[h]
R9	FAME2 + H = FAME2MJ + H_2	4.35×10^{4}	2.83	6.75×10^{3}	[h]
R10	FAME2 + CH_3 = FAME2MJ + CH_4	5.92×10^{-1}	3.70	6.82×10^{3}	[i]
R11	FAME2 + H = FA2 + CH_3	7.41×10^{21}	−1.92	1.96×10^{4}	[i]
R12	FAME2 + H = f2cho + CH_3O	1.24×10^{21}	−1.92	1.96×10^{4}	[j]
R13	FAME2 + H = furan + CH_3OCO	2.47×10^{21}	−1.92	1.96×10^{4}	[k]
R14	FAO2J + H = FA2	1.00×10^{14}	0.00	0.00	[l]
R15	FAO2J = f2j + CO_2	1.61×10^{15}	0.09	1.64×10^{4}	[m]
R16	FAME2MJ = f2cjo + CH_2O	5.60×10^{12}	0.63	1.51×10^{4}	[n]
R17	f2cjo = f2j + CO	4.00×10^{14}	0.00	2.95×10^{4}	20
R18	f2j = CH═CHCH═C═O	1.80×10^{13}	0.34	3.45×10^{4}	20
R19	C_2H_2 + HCCO = CH═CHCH═C═O	1.61×10^{40}	−8.58	2.03×10^{4}	20
R20	CH═CHCH═C═O = CH≡CCH═C═O + H	8.72×10^{11}	0.71	3.87×10^{4}	20
R21	CH≡CCH═C═O + H = CO + C_3H_3	1.54×10^{14}	−0.17	4.18×10^{3}	20
R22	C_2H_2 + HCCO = CO + C_3H_3	2.00×10^{11}	0.00	3.00×10^{3}	20
R23	p23de5o1ooch3-t = $C_5H_6O_2$-3 + CO	3.45×10^{18}	−1.46	4.90×10^{4}	[o]
R24	p34de2o1ooch3-t═CH_2═C═CHCO + CH_3OCO	1.80×10^{14}	0.00	2.94×10^{4}	[p]
R25	CH_3OCO = CO_2 + CH_3	1.89×10^{9}	0.13	7.97×10^{3}	6
R26	CH_3OCO = CO + CH_3O	6.11×10^{-2}	2.95	1.78×10^{4}	6
R27	CH_2CO + H ⇔ HCCO + H_2	1.41×10^{15}	−0.17	8.78×10^{3}	20
R28	CH_2O + CH_3 ⇔ HCO + CH_4	3.88×10^{1}	3.36	4.31×10^{3}	20

[a]Rate coefficients are given as $k = AT^n\exp(-E_a/RT)$. Units are in s^{-1}, cm^3, and cal/mol, respectively. [b]Analogy with MC = CH_3CH═CHC(O)O + CH_3, reaction rate rule from ref 12. [c]Assumed rate rule for the cleavage of side chain from ref 7. [d]Assumed rate rule for the cleavage of side chain from ref 21. [e]Analogy with CH_3OCHO = CH_2O + CH_2O, reaction rate rule from ref 48. [f]Analogy with CH_3OCHO = CH_4 + CO_2, reaction rate rule from ref 49. [g]Analogy with CH_3OCHO = CH_3OH + CO, reaction rate rule from ref 49. [h]Analogy with H-shift reactions of MF from ref 21. [i]Assumed rate rule for abstraction of primary H-atom from ref 6. [j]Analogy with substitution of MF by H-atom from ref 21. [k]Analogy with H-addition reaction of MF from ref 21. [l]Analogy with HCOO + H = HCOOH from ref 50. [m]Analogy with $CH_3OC(O)O$ = CH_3O + CO_2 from ref 6. [n]Analogy with $CH_3OC(O)OCH_2$ = CH_2O + CH_3OCO from ref 6. [o]Analogy with $CH_3CHCCHCHO$-t = CO + C_4H_6-1 from ref 21. [p]Analogy with $CH_3OCOCOOCH_3$ = CH_3OCO + CH_3OCO from ref 51.

10^{-1} to 1.62×10^{-1} s with its corresponding temperature range at 760 Torr, and the calculated Reynolds number (Re) of the flow is always less than 2000 when T_{max} varied from 879 - 1107 K.

Uncertainties of the mole fractions mainly came from the photoionization cross sections (PICSs) and were estimated to be around ±25% for those species with known PICSs and a factor of 2 for those with estimated PICSs. The PICSs data adopted in this work are available in the online Photonionization Crosss Section Database.[42] The PICSs of FAME2 were measured in this work because of the lack of the reported data.

3. THEORETICAL METHODS AND KINETIC MODEL

3.1. Theoretical Calculations. All the quantum chemistry calculation was conducted by using the Gaussian 09 program.[43] The M06-2X density functional method with the cc-pVTZ basis set, followed by the highly precise CBS-QB3 method to calculate the single point energy, was employed in geometry optimization of reactants, transition states, intermediates, and products. Transition states were verified as those possessing a reasonable geometry with only one imaginary frequency, whose atomic displacement appeared to approximate the desired reaction coordinate via visual inspections. The ionization energy (IE) of important intermediates was computed by using the CBS-QB3 compound method.

3.2. Kinetic Model. In this work, simulation of FAME2 pyrolysis was performed using the plug flow reactor code in Chemkin Pro software.[44] A detailed kinetic model of FAME2 pyrolysis including 601 species and 3086 reactions is developed, and the input files of thermodynamic data and gas-phase kinetics are available in the Supporting Information. The submechanism of FAME2 was developed and added into the updated combustion model of furanic fuels by Cheng et al.[20,22,23] based on Somers model,[21] where the C0−C4 submechanism was proposed by Curran and co-workers in their recent study.[45] The key reactions in FAME2 submechanism are listed in Table 1 with the corresponding Arrhenius parameters at 760 Torr. Rate coefficients for some key reactions are evaluated as described below. The molecular weights, formulas, names, nomenclatures in the present model, and structures are listed in Table S1 in the Supporting Information. Because of the lack of theoretical and experimental investigations for the complex structure of FAME2, the rate coefficients of FAME2 decomposition are assumed by analogy with the similar reactions of CH_3OCHO, DMC, MC and furan, MF, DMF. The construction of the FAME2 submechanism is described in detail below. Thermodynamic data of all species in the present model were derived from the previous models[20,21,46] or calculated by the THERGAS program.[47]

Decomposition of FAME2 in the pyrolysis process was controlled by unimolecular decomposition reactions, H-addition reactions, H-abstraction reactions, and substitution reactions. The unimolecular decomposition on the ester group of FAME2 can decompose to 2-furoyloxyl (FAOJ2) + CH_3, 2-furoyl radical (f2cjo) + methoxy (CH_3O), and 2-furyl radical (f2j) + CH_3OCO. Elimination reactions can produce f2cho + formaldehyde (CH_2O), MF + CO_2, and 2-

DOI: 10.1021/acs.energyfuels.9b00367
Energy Fuels 2019, 33, 4611−4620

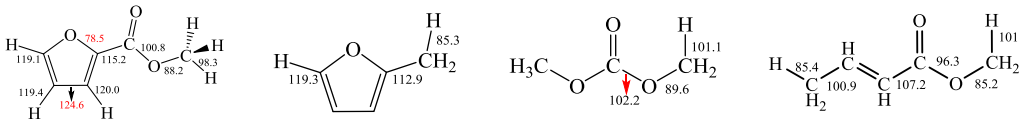

Figure 2. Schematic structures of FAME2, MF,[17] DMC,[52] and MC.[53] The numbers refer to BDEs in the unit of kcal/mol. The BDEs of FAME2 were calculated at the CBS-QB3 level in this work.

methoxyfuran (f2och3) + CO (R4−R6). The reaction rate constants of R1, R2, and R3 were estimated based on the reaction rate constants of MC,[12] MP[7], and MF[21] decomposition, respectively, because the corresponding bond energies of C(O)O−CH_3, C(O)−OCH_3, and C(2)−C(O)OCH_3 bonds in FAME2 are similar to those of the three esters, as shown in Figure 2. As to R4, R5, and R6, the reaction rate constants were estimated by analogy with the reactions CH_3OCHO = CH_2O + CH_2O,[48] CH_3OCHO = CH_4 + CO_2,[49] and CH_3OCHO = CH_3OH + CO,[49] respectively. FAME2 may also be consumed by opening the furan ring via H-migration reactions, analogous to those in the pyrolysis of MF, to produce methyl 5-oxo-2,3-pentadienoate (OHCCH═C═CHCOOCH_3, p23de5o1ooch3-t) (R7) and methyl 2-oxo-3,4-pentadienoate (CH_2═C═CHCOCOOCH_3, p34de2o1ooch3-t) (R8). The reaction constants of R7 and R8 were estimated based on similar reactions of MF = CH_3CHCCHCHO-t and MF = CH_3COCHCCH_2-t proposed by Somers et al.[21]

The H-atom abstraction reactions of FAME2 by H/CH_3 can produce 2-furoyloxylmethyl (FAME2MJ) (R9 and R10). The bond dissociation energies (BDEs) of a number of similar fuels reported in the literature are also displayed in Figure 2. In the current model, the rate constants of R9 and R10 were estimated by analogy with the similar reaction of DMC from Sun et al.[6] The rate constants were divided by a factor of 2 in the current model, given the single CH_3 group in FAME2 other than the two CH_3 groups in DMC. Substitution reactions of FAME2 by the H-atom can produce FA2 + CH_3 and CH_3O + f2cho (R11 and R12). The rate constants of R11 and R12 were estimated from the analogous reaction of MF + H = furan + CH_3 calculated by Somers et al.[21] Because the BDE of C(O)O−CH_3 (88.2 kcal/mol) in FAME2 is lower than that of C−CH_3 (112.9 kcal/mol) in MF, R11 should be much faster than the reaction of MF + H = furan + CH_3. In comparison to adjust E_a, the simpler method to change the rate by adjusting the preexponential factor is adopted. Hence, the pre-exponential factor was multiplied by 3 for R11 to better simulate the pyrolysis of FAME2. The rate constant of R13 was estimated by analogy with the reaction of MF + H = furan + CH_3.

The rate constants of R14, R15, and R16 were adopted by analogy to the similar reactions of HCOO + H = HCOOH,[50] $CH_3OC(O)O$ = CH_3O + CO_2,[6] and $CH_3OC(O)OCH_2$ = CH_2O + CH_3OCO,[6] respectively. As to R17−R22 and R27−R28, the constants adopted in the current mechanism came from the model of Cheng et al.[20] The rate constants of R23 and R24 were assumed by analogy to the similar reactions of CH_3CHCCHCHO-t = CO + C_4H_6-1[21] and $CH_3OCOCOOCH_3$ = CH_3OCO + CH_3OCO,[51] respectively. The rate constants of R25 and R26 were calculated by Sun et al.[6]

4. RESULTS AND DISCUSSION

Thirty pyrolysis species, including isomers, and important intermediates were identified, and 21 of them with respective mole fraction profiles as a function of temperature were measured, as shown in Figures 4−6. The present kinetic model was validated against the current pyrolysis experimental results.

The photoionization efficiency (PIE) spectra of m/z = 126 and m/z = 112 for photon energies ranging from 8.5 to 11.0 eV are shown in Figure 3. The experimental and simulated mole fraction profiles of FAME2 and its pyrolysis products at 760 Torr are shown in Figures 4−6. The calculated major decomposition pathways of FAME2 at the CBS-QB3 level

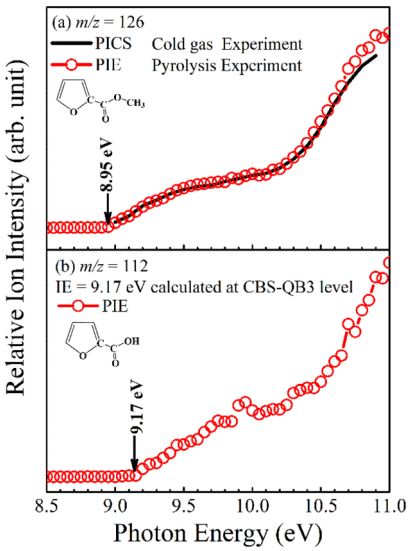

Figure 3. PIE of the species (a) m/z = 126 and (b) m/z = 112 in the cold gas experiment and pyrolysis experiment of FAME2.

are shown in Figure 7. On the basis of ROP analysis, the reaction networks of FAME2 pyrolysis at 1082 K and 760 Torr are summarized in Figure 8. At this temperature, about 78% of FAME2 is consumed and most products reach relatively high concentration levels. The sensitivity analysis of FAME2 decomposition at 1082 K is displayed in Figure 9 to demonstrate the most sensitive reactions to FAME2 pyrolysis at atmospheric pressure.

4.1. Identification of Pyrolysis Species. In this work, the pyrolysis species are identified by the molecular weight and the corresponding IE measured from the photoionization mass spectrum and PIE spectra, respectively. The identification of m/z = 126 and m/z = 112 will be discussed in detail herein. Other products measured in this experiment are listed in Table S2 in the Supporting Information.

Figure 3a shows the onset at 8.95 eV on the PIE corresponding to the reported IE of FAME2 (9.00 ± 0.05 eV[54]). This PIE is in good agreement with that of pure FAME2 measured in this work. Thus, the species of m/z = 126 is identified as FAME2. The PIE of pure FAME2 was measured by scanning the mixture of FAME2 and nitric oxide (NO) with a molar ratio of 1:2 at the photon energy of 9.00−15.00 eV and T = 1048 K, p = 30 Torr. NO was used in the measurements as a calibrator with its well-known PICS at the photon energies of 9.22−15.00 eV.[55] The PICS of FAME2 can be obtained from the PIE in the cold gas experiment by eq 1[56−58]

$$\frac{S_T}{S_S} = \frac{X_T \cdot \sigma_T(E) \cdot R_T}{X_S \cdot \sigma_S(E) \cdot R_S} \quad (1)$$

where the subscripts T and S stand for target and standard samples, respectively; $\sigma(E)$ is the PICS at the photon energy of

DOI: 10.1021/acs.energyfuels.9b00367
Energy Fuels 2019, 33, 4611−4620

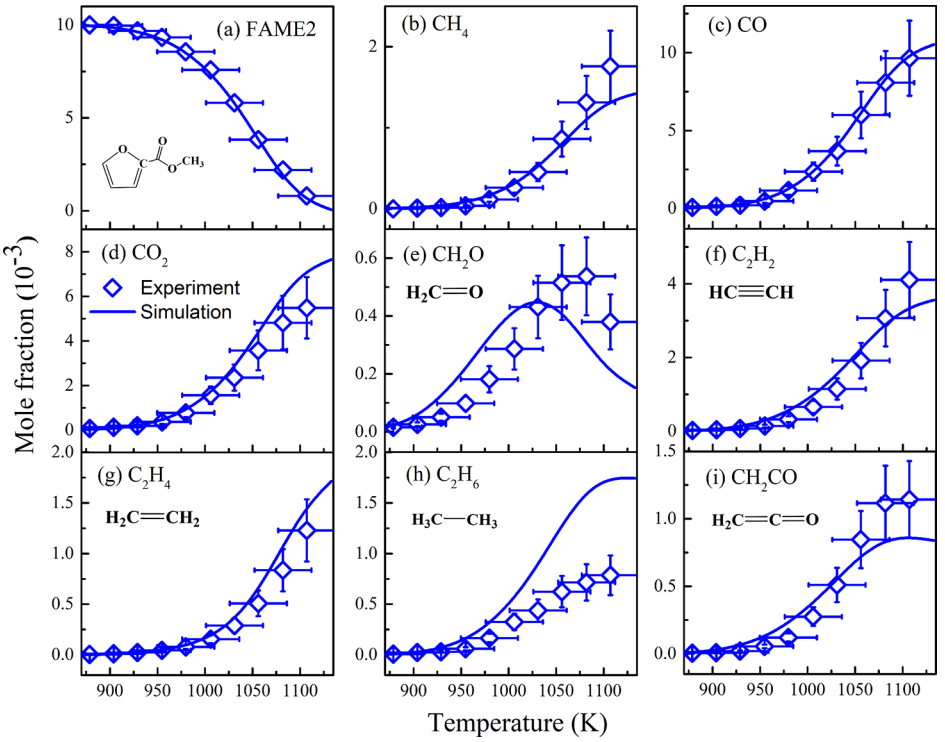

Figure 4. Experimental (symbols) and simulated (lines) mole fraction profiles of FAME2, methane (CH_4), carbon monoxide (CO), carbon dioxide (CO_2), formaldehyde (CH_2O), acetylene (C_2H_2), ethene (C_2H_4), ethane (C_2H_6), and ketene (CH_2CO) in FAME2 pyrolysis at 760 Torr.

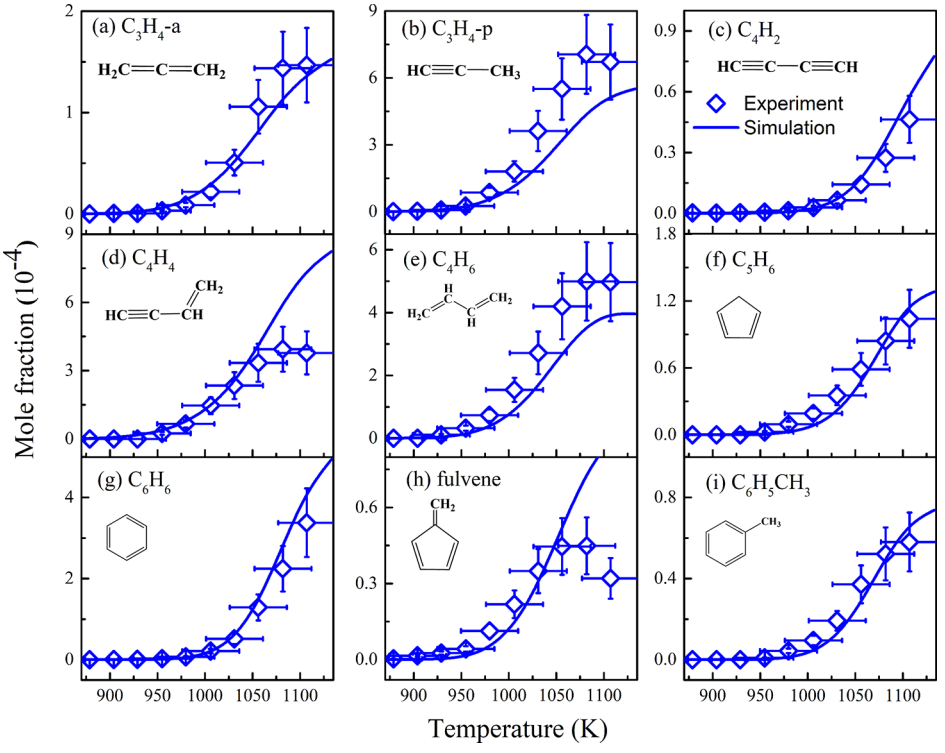

Figure 5. Experimental (symbols) and simulated (lines) mole fraction profiles of allene (C_3H_4-a), propyne (C_3H_4-p), diacetylene (C_4H_2), vinylacetylene (C_4H_4), 1,3-butadiene (C_4H_6), cyclopentene (C_5H_6), benzene (C_6H_6), fulvene, and toluene ($C_6H_5CH_3$) in FAME2 pyrolysis at 760 Torr.

E eV; *R* is the mass discrimination factor; *X* is the mole fraction; and *S* is the signal intensity.

The species of m/z = 112 may be 1,3,5,7-nonantetrayne (C_9H_4, IE = 8.68 eV[42]) or FA2 (IE = 9.17 eV, calculated in this work). Figure 3b shows that there is an obvious onset at 9.17 eV on the PIE corresponding to the calculated IE of FA2. Thus, the species of m/z = 112 is identified as FA2, instead of C_9H_4.

DOI: 10.1021/acs.energyfuels.9b00367
Energy Fuels 2019, 33, 4611−4620

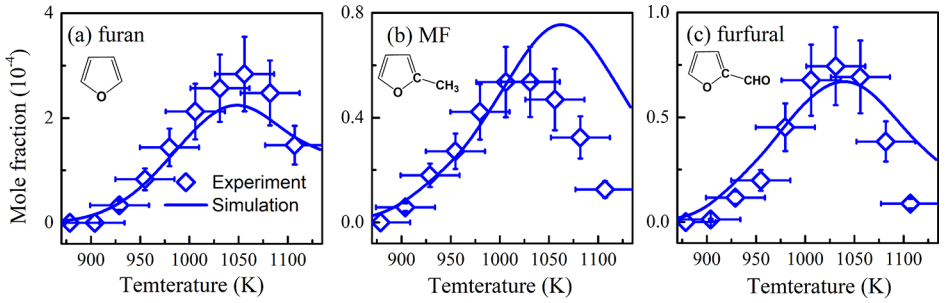

Figure 6. Experimental (symbols) and simulated (lines) mole fraction profiles of furan, MF, and f2cho in FAME2 pyrolysis at 760 Torr.

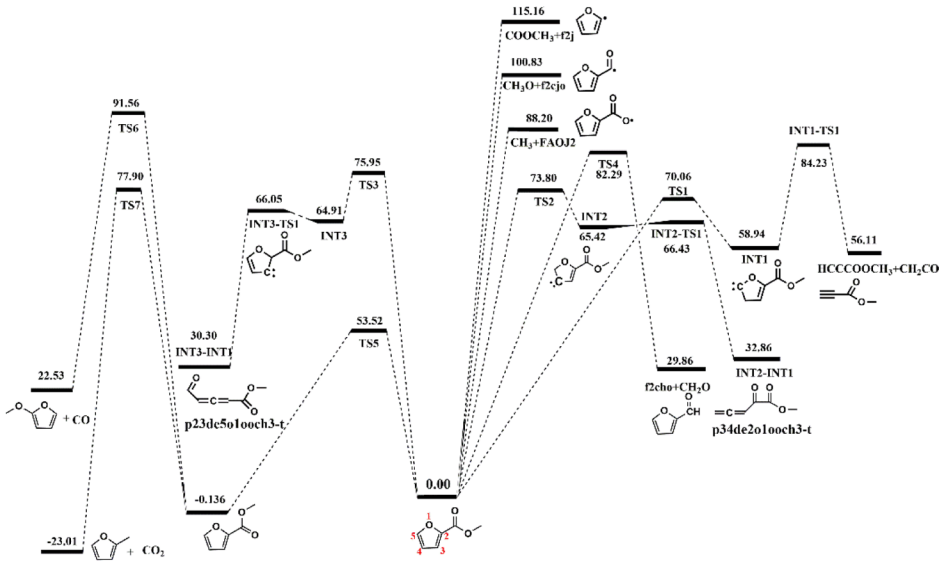

Figure 7. Calculated major decomposition pathways of FAME2 at the CBS-QB3 level. The energies (in kcal/mol) with zero-point-energy correction are relative to FAME2.

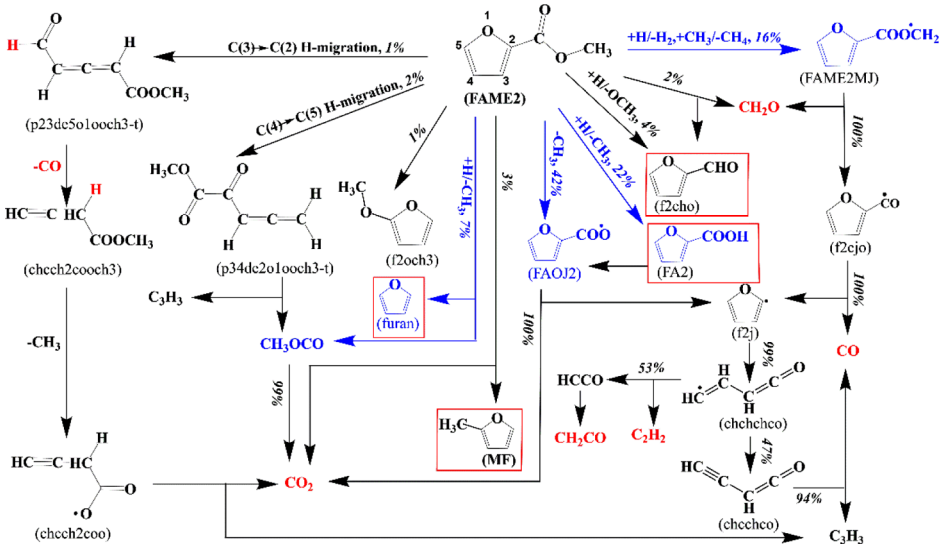

Figure 8. Primary pyrolysis reaction pathways of FAME2 at 78% consumption.

4.2. Decomposition Pathways. Figures 4–6 show that the present model can reproduce the experimental results reasonably, including the decomposition temperature of FAME2, the appearance temperature of the products, and the mole fraction profiles of the major species. In general, ROP analysis shows that FAME2 is mainly consumed by four types of reactions, that is, unimolecular decomposition reactions, substitution reactions by H-atom, H-atom abstraction reactions by H/CH_3 radicals, and H-addition reaction.

Theoretical calculations at the CBS-QB3 level, as shown in Figure 7, indicate that FAME2 can be consumed by three types of unimolecular decomposition reactions, direct decomposi-

DOI: 10.1021/acs.energyfuels.9b00367
Energy Fuels 2019, 33, 4611−4620

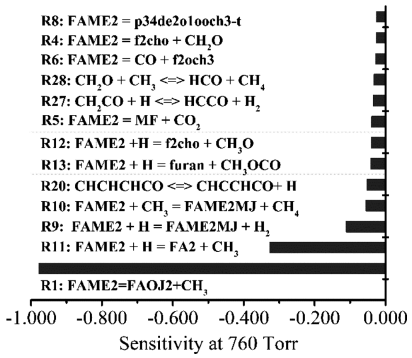

Figure 9. Sensitivity analysis of FAME2 pyrolysis at 1082 K and 760 Torr.

tion of FAME2 by breaking the corresponding bonds (R1−R3), molecular elimination reactions (R4−R6), and unimolecular isomerizations (R7 and R8) via cyclic carbenes produced by the corresponding H-migration.

Similar to most esters,[6,7,12,28,59] the breakage of C(O)O−CH_3 bond in FAME2 (R1) plays a critical role in the pyrolysis and contributes substantially to FAME2 consumption at 760 Torr. The reaction pathway analysis shows that about 42% consumption of FAME2 is controlled by R1. This point is in agreement with the decomposition pathways calculated at the CBS-QB3 level. The breakage of C(O)−OCH_3 bond in FAME2 (R2) leads to the formation of f2cjo, whereas the direct cleavage of C(2)−C(O)OCH_3 bond of the fuel (R3) produces CH_3OCO. R2 and R3 are found to be uncompetitive with R1, possibly because of the higher energy barriers of R2 and R3 (100.83 and 115.16 kcal/mol, respectively) than that of R1 (88.20 kcal/mol) encountered on their PESs. Subsequent decomposition reaction of FAOJ2 (R15) dominates the formation of f2j and CO_2. ROP analysis indicates that about 84% formation of CO_2 is controlled by R15, and 12% formation of CO_2 is controlled by CH_3OCO decomposition (R25). The decomposition reaction of f2cjo (R17) can produce f2j and CO. CO can also be produced by R19 and R21 in FAME2 pyrolysis. f2j is produced by R15 and R17 and subsequently decomposes to CH═CHCH═C═O by opening the furan ring (R18). Breakage of C−C bond in CH═CHCH═C═O produces C_2H_2 + HCCO (R19), playing a key role in C_2H_2 and CH_2CO formation. Another consumption pathway of CH═CHCH═C═O is to produce CH≡CCH═C═O by β-C−H bond cleavage (R20). C_3H_3 radicals, the significant precursor for C_3H_4-a, C_3H_4-p, C_4H_2, C_4H_4, C_6H_6, and fulvene, are generated by R21 and R22. Another three elimination reactions of R4−R6 have a relatively slight contribution (6%) to the consumption of FAME2. Although the energy barrier of R1 in Figure 7 is relatively higher than R4, it contributes higher to the consumption of FAME2 than R4 does, according to the ROP analysis. This can be attributed to the different natures of the two reactions, with R1 producing two radicals (f2cjo and CH_3) and R4 producing two stable species (f2cho and CH_2O). Radicals are active and hence accelerate the progress of R1. According to the ROP analysis, f2cho is produced by R4 (29%) and R12 (71%). It is worth mentioning that R5 and R6 are the major formation pathway of MF and f2och3, respectively.

Besides the reactions on the ester groups of FAME2, the opening of the furan ring via H-migration reactions (R7 and R8) also contributes to the consumption of FAME2 substantially. However, only about 3% of FAME2 is consumed by H-migration reactions, a lower contribution than the analogous H-migration reactions in MF pyrolysis as reported by Cheng et al.[22] at 760 Torr. It may be attributed to the fact that the CH_3OCO group in FAME2 is larger than the CH_3 group in MF and the presence of C═O double bond in the CH_3OCO group and C(2)═C(3) in the furyl. The above two points make H-migration reactions less favorable in FAME2. In the unimolecular isomerization pathways of FAME2, a H-atom migrates from C(3) to C(2) (R7) or from C(4) to C(5) (R8) to produce the corresponding cyclic carbenes. According to the similar case in MF pyrolysis,[21] the H-migration from C(5) to C(4) is uncompetitive to R7 or R8 and will not be discussed in this work. Theoretical calculations also confirm this point, as shown in Figure 7, where the activation energy of C(5)−H migration is much higher than that of C(4)−H transfer. For R7, the H-atom on C(3) migrates to C(2) to form the corresponding carbene and then isomerizes to p23de5o1ooch3-t. Subsequent decomposition of p23de5o1ooch3-t may lead to the formation of methyl 3-butynoate (HC≡CCH_2COOCH_3, $C_5H_6O_2$-3) and CO (R22), analogous to that of CH_3CHCCHCHO-t (CH_3CH═C═CHCHO) in MF pyrolysis.[21,22] For R8, the H-atom on C(4) migrates to C(5) to form the β-carbene and then isomerizes to p34de2o1ooch3-t. Subsequent decomposition of p34de2o1ooch3-t leads to the formation of H_2C═C═CHCO and CH_3OCO (R24), analogous to that in dimethyl oxalate ($C_4H_6O_4$)[51] decomposition. In fact, the C(1)−C(2) bond should be the weakest in p34de2o1ooch3-t because of the two adjacent carbonyls.

Substitution reactions of FAME2 by the H-atom (R11 and R12) are considered because of the lower BDEs in C(O)O−CH_3 and C(O)−OCH_3. The ROP analysis shows that about 26% of FAME2 is consumed by R11 and R12. R11 is the only pathway to form FA2, which is subsequently decomposed by R14, and also plays a vital role in the progress of CH_3 formation except R1. CH_3 is consumed by the self-combination reaction of CH_3 (CH_3 + CH_3 = C_2H_6) to produce C_2H_6, which is a dominant pathway for C_2H_6 formation. The H-atom abstraction reactions of FAME2 by H/CH_3 (R9 and R10), which contribute substantially (about 16%) to the consumption of FAME2, can produce FAME2MJ which can be decomposed into f2j and CH_2O (R16). About 7% of FAME2 is consumed by the H-addition reaction (R13), which is also a critical pathway for furan formation.

The sensitivity analysis of FAME2 can reveal the influences of the unimolecular decomposition, substitution by H-atom, H-abstraction, and H-addition reactions on the consumption of FAME2 at 760 Torr. It is observed that the unimolecular decomposition pathway (R1) and substitution reaction by H-atom (R11) are sensitive to FAME2 consumption at atmospheric pressure. The sensitivity analysis is in accordance with the calculated major unimolecular decomposition pathways of FAME2 at the CBS-QB3 level, as displayed in Figure 7. Meanwhile, R1, R5, R9, R11, R12, and R13 are closely related with the formation of the key species, such as CO_2, CO, CH_2O, furan, MF, f2cho, FA2, and so forth.

On the basis of the above discussion, unimolecular decomposition, substitution by H-atom, H-abstraction, and H-addition reactions should play key roles in the pyrolysis of FAME2 and the formation of products, such as CO, CO_2, CH_2O, C_2H_2, C_2H_6, CH_2CO, C_3H_4-a, C_3H_4-p, C_4H_2, C_4H_4, C_5H_6, C_6H_6, furan, MF, and f2cho. Similar to most oxygenated

DOI: 10.1021/acs.energyfuels.9b00367
Energy Fuels 2019, 33, 4611−4620

fuels,[5,6,28] there are relatively few aromatics in the pyrolysis of FAME2. The experimental and simulated mole fraction profiles of C_6H_6, fulvene, and $C_6H_5CH_3$ are shown in Figure 5g–i. In the future, more detailed and precise theoretical calculation pathways and more experimental studies at various pressures should be performed to improve the accuracy of the kinetic model, and the pathways of PAHs formation should be clarified.

5. CONCLUSIONS

Experimental studies of FAME2 pyrolysis were performed in a flow reactor from 879 to 1107 K at 760 Torr. About 21 species were identified and measured, especially several important intermediates. A kinetic model was proposed by analogy to those of similar fuels. In general, the present model can reproduce the experimental results of most pyrolysis species within the experimental uncertainties. The ROP analysis and sensitivity analysis were performed to analyze the main reaction pathways in the pyrolysis of FAME2. Decomposition of FAME2 in pyrolysis is initiated by the unimolecular decomposition pathways, including the release of CH_3 from FAME2, elimination reactions by certain molecular, and the unimolecular isomerization pathways of FAME2 by H-migration reactions, producing methyl + 2-furoyloxyl radicals and methyl 5-oxo-2,3-pentadienoate + methyl 2-oxo-3,4-pentadienoate, respectively. Substitution by H-atom and H-abstraction reactions are also vital to the consumption of FAME2. The formation reaction pathways of important intermediates, including f2cho, furoic acid, 2-methylfuran, furan, etc., were also proposed and discussed. The ROP analysis shows that substitution reactions by the H-atom dominate the formation of f2cho and furoic acid, CO_2 molecular elimination reaction controls the formation of 2-methylfuran, and H-addition reaction is the crucial pathway to produce furan. Formation of aromatics is undetectable in the pyrolysis of FAME2.

■ ASSOCIATED CONTENT

Supporting Information

The Supporting Information is available free of charge on the ACS Publications website at DOI: 10.1021/acs.energyfuels.9b00367.

Chemical structures and nomenclature of some species involved in the methyl furoate pyrolysis and list of intermediates measured in the pyrolysis of FAME2 (PDF)

Temperature profiles (XLSX)

Reaction mechanism (TXT)

Thermodynamic data (TXT)

■ AUTHOR INFORMATION

Corresponding Authors

*E-mail: zjcheng@tju.edu.cn. Phone: +86-22-87401929 (Z.C.).

*E-mail: feilix@gxu.edu.cn. Phone: +86-13197510423 (L.W.).

ORCID

Beibei Yan: 0000-0003-0499-8712

Zhanjun Cheng: 0000-0002-7480-5413

Jiuzhong Yang: 0000-0002-7076-3412

Notes

The authors declare no competing financial interest.

■ ACKNOWLEDGMENTS

The authors thank the funding supports from the National Natural Science Foundation of China (nos. 51776045, 51506143, and 51676138), the Project Sponsored by the Scientific Research Foundation of Guangxi University (grant no. XGZ170074), National Key R&D Program of China (2016YFE0201800), and Tianjin Research Program of Application and Advanced Technology (16JCZDJC39600). The authors thank Dr. Lili Ye and Dr. Lidong Zhang for their kind help.

■ ABBREVIATIONS

FAME2 = methyl 2-furoate
CH_3OCHO = methyl formate
DMC = dimethyl carbonate
MP = methyl propionate
MB = methyl butanoate
MC = methyl crotonate
MF = 2-methylfuran
DMF = 2,5-dimethylfuran
FA2 = 2-furoic acid
f2cho = furfural
PES = potential energy surface
IE = ionization energy
BDEs = bond dissociation energies
PIE = photoionization efficiency
SVUV-PIMS = synchrotron vacuum ultraviolet photoionization mass spectrometry
PICSs = photoionization cross sections
ROP = rate of production

■ REFERENCES

(1) Acheampong, M.; Ertem, F. C.; Kappler, B.; Neubauer, P. In pursuit of Sustainable Development Goal (SDG) number 7: Will biofuels be reliable? *Renewable Sustainable Energy Rev.* **2017**, *75*, 927–937.

(2) Aransiola, E. F.; Ojumu, T. V.; Oyekola, O. O.; Madzimbamuto, T. F.; Ikhu-Omoregbe, D. I. O. A review of current technology for biodiesel production: State of the art. *Biomass Bioenergy* **2014**, *61*, 276–297.

(3) Azadi, P.; Malina, R.; Barrett, S. R. H.; Kraft, M. The evolution of the biofuel science. *Renewable Sustainable Energy Rev.* **2017**, *76*, 1479–1484.

(4) Nigam, P. S.; Singh, A. Production of liquid biofuels from renewable resources. *Prog. Energy Combust. Sci.* **2011**, *37*, 52–68.

(5) Ren, W.; Dames, E.; Hyland, D.; Davidson, D. F.; Hanson, R. K. Shock tube study of methanol, methyl formate pyrolysis: CH3OH and CO time-history measurements. *Combust. Flame* **2013**, *160*, 2669–2679.

(6) Sun, W.; Yang, B.; Hansen, N.; Westbrook, C. K.; Zhang, F.; Wang, G.; Moshammer, K.; Law, C. K. An experimental and kinetic modeling study on dimethyl carbonate (DMC) pyrolysis and combustion. *Combust. Flame* **2016**, *164*, 224–238.

(7) Zhao, L.; Xie, M.; Ye, L.; Cheng, Z.; Cai, J.; Li, Y.; Qi, F.; Zhang, L. An experimental and modeling study of methyl propanoate pyrolysis at low pressure. *Combust. Flame* **2013**, *160*, 1958–1966.

(8) Akih-Kumgeh, B.; Bergthorson, J. M. Structure-reactivity trends of C1–C4 alkanoic acid methyl esters. *Combust. Flame* **2011**, *158*, 1037–1048.

(9) Gaïl, S.; Sarathy, S. M.; Thomson, M. J.; Diévart, P.; Dagaut, P. Experimental and chemical kinetic modeling study of small methyl esters oxidation: Methyl (E)-2-butenoate and methyl butanoate. *Combust. Flame* **2008**, *155*, 635–650.

DOI: 10.1021/acs.energyfuels.9b00367
Energy Fuels 2019, 33, 4611–4620

(10) Garner, S.; Brezinsky, K. Biologically derived diesel fuel and NO formation: An experimental and chemical kinetic study, Part 1. *Combust. Flame* **2011**, *158*, 2289−2301.
(11) Wang, W.; Oehlschlaeger, M. A. A shock tube study of methyl decanoate autoignition at elevated pressures. *Combust. Flame* **2012**, *159*, 476−481.
(12) Zhai, Y.; Feng, B.; Yuan, W.; Ao, C.; Zhang, L. Experimental and modeling studies of small typical methyl esters pyrolysis: Methyl butanoate and methyl crotonate. *Combust. Flame* **2018**, *191*, 160−174.
(13) Zhou, X.; Zhai, Y.; Ye, L.; Zhang, L. Theoretical studies on the reaction kinetics of methyl crotonate with hydroxyl radical. *Sustainable Energy Fuels* **2018**, *2*, 392−402.
(14) Zhai, Y.; Ao, C.; Feng, B.; Meng, Q.; Zhang, Y.; Mei, B.; Yang, J.; Liu, F.; Zhang, L. Experimental and kinetic modeling investigation on methyl decanoate pyrolysis at low and atmospheric pressures. *Fuel* **2018**, *232*, 333−340.
(15) Román-Leshkov, Y.; Barrett, C. J.; Liu, Z. Y.; Dumesic, J. A. Production of dimethylfuran for liquid fuels from biomass-derived carbohydrates. *Nature* **2007**, *447*, 982.
(16) Liu, D.; Togbé, C.; Tran, L.-S.; Felsmann, D.; Oßwald, P.; Nau, P.; Koppmann, J.; Lackner, A.; Glaude, P.-A.; Sirjean, B.; Fournet, R.; Battin-Leclerc, F.; Kohse-Höinghaus, K. Combustion chemistry and flame structure of furan group biofuels using molecular-beam mass spectrometry and gas chromatography—Part I: Furan. *Combust. Flame* **2014**, *161*, 748−765.
(17) Togbé, C.; Tran, L.-S.; Liu, D.; Felsmann, D.; Oßwald, P.; Glaude, P.-A.; Sirjean, B.; Fournet, R.; Battin-Leclerc, F.; Kohse-Höinghaus, K. Combustion chemistry and flame structure of furan group biofuels using molecular-beam mass spectrometry and gas chromatography—Part III: 2,5-Dimethylfuran. *Combust. Flame* **2014**, *161*, 780−797.
(18) Tran, L.-S.; Togbé, C.; Liu, D.; Felsmann, D.; Oßwald, P.; Glaude, P.-A.; Fournet, R.; Sirjean, B.; Battin-Leclerc, F.; Kohse-Höinghaus, K. Combustion chemistry and flame structure of furan group biofuels using molecular-beam mass spectrometry and gas chromatography—Part II: 2-Methylfuran. *Combust. Flame* **2014**, *161*, 766−779.
(19) Banerjee, A.; Dick, G. R.; Yoshino, T.; Kanan, M. W. Carbon dioxide utilization via carbonate-promoted C−H carboxylation. *Nature* **2016**, *531*, 215.
(20) Cheng, Z.; Tan, Y.; Wei, L.; Xing, L.; Yang, J.; Zhang, L.; Guan, Y.; Yan, B.; Chen, G.; Leung, D. Y. C. Experimental and kinetic modeling studies of furan pyrolysis: Fuel decomposition and aromatic ring formation. *Fuel* **2017**, *206*, 239−247.
(21) Somers, K. P.; Simmie, J. M.; Metcalfe, W. K.; Curran, H. J. The pyrolysis of 2-methylfuran: a quantum chemical, statistical rate theory and kinetic modelling study. *Phys. Chem. Chem. Phys.* **2014**, *16*, 5349−5367.
(22) Cheng, Z.; He, S.; Xing, L.; Wei, L.; Li, W.; Li, T.; Yan, B.; Ma, W.; Chen, G. Experimental and Kinetic Modeling Study of 2-Methylfuran Pyrolysis at Low and Atmospheric Pressures. *Energy Fuels* **2017**, *31*, 896−903.
(23) Cheng, Z.; Niu, Q.; Wang, Z.; Jin, H.; Chen, G.; Yao, M.; Wei, L. Experimental and kinetic modeling studies of low-pressure premixed laminar 2-methylfuran flames. *Proc. Combust. Inst.* **2017**, *36*, 1295−1302.
(24) Cheng, Z.; Xing, L.; Zeng, M.; Dong, W.; Zhang, F.; Qi, F.; Li, Y. Experimental and kinetic modeling study of 2,5-dimethylfuran pyrolysis at various pressures. *Combust. Flame* **2014**, *161*, 2496−2511.
(25) Xu, N.; Tang, C.; Meng, X.; Fan, X.; Tian, Z.; Huang, Z. Experimental and Kinetic Study on the Ignition Delay Times of 2,5-Dimethylfuran and the Comparison to 2-Methylfuran and Furan. *Energy Fuels* **2015**, *29*, 5372−5381.
(26) Xu, N.; Wu, Y.; Tang, C.; Zhang, P.; He, X.; Wang, Z.; Huang, Z. Experimental study of 2,5-dimethylfuran and 2-methylfuran in a rapid compression machine: Comparison of the ignition delay times and reactivity at low to intermediate temperature. *Combust. Flame* **2016**, *168*, 216−227.
(27) Eldeeb, M. A.; Akih-Kumgeh, B. Reactivity Trends in Furan and Alkyl Furan Combustion. *Energy Fuels* **2014**, *28*, 6618−6626.
(28) Ning, H.; Wu, J.; Ma, L.; Ren, W.; Davidson, D. F.; Hanson, R. K. Chemical kinetic modeling and shock tube study of methyl propanoate decomposition. *Combust. Flame* **2017**, *184*, 30−40.
(29) Gaïl, S.; Thomson, M. J.; Sarathy, S. M.; Syed, S. A.; Dagaut, P.; Diévart, P.; Marchese, A. J.; Dryer, F. L. A wide-ranging kinetic modeling study of methyl butanoate combustion. *Proc. Combust. Inst.* **2007**, *31*, 305−311.
(30) Wei, L.; Tang, C.; Man, X.; Jiang, X.; Huang, Z. High-Temperature Ignition Delay Times and Kinetic Study of Furan. *Energy Fuels* **2012**, *26*, 2075−2081.
(31) Grela, M. A.; Amorebieta, V. T.; Colussi, A. J. Very Low Pressure Pyrolysis of Furan, 2-Methylfuran, and 2,5-Dimethylfuran. The Stability of the Furan Ring. *J. Phys. Chem. A* **1985**, *89*, 38−41.
(32) Lifshitz, A.; Bidani, M.; Bidani, S. Thermal reactions of cyclic ethers at high temperatures. III. Pyrolysis of furan behind reflected shocks. *J. Phys. Chem. A* **1986**, *90*, 5373−5377.
(33) Lifshitz, A.; Tamburu, C.; Shashua, R. Decomposition of 2-methylfuran. Experimental and modeling study. *J. Phys. Chem. A* **1997**, *101*, 1018−1029.
(34) Lifshitz, A.; Tamburu, C.; Shashua, R. Thermal decomposition of 2,5-dimethylfuran. Experimental results and computer modeling. *J. Phys. Chem. A* **1998**, *102*, 10655−10670.
(35) Tian, Z.; Pitz, W. J.; Fournet, R.; Glaude, P.-A.; Battin-Leclerc, F. A detailed kinetic modeling study of toluene oxidation in a premixed laminar flame. *Proc. Combust. Inst.* **2011**, *33*, 233−241.
(36) Sirjean, B.; Fournet, R.; Glaude, P.-A.; Battin-Leclerc, F.; Wang, W.; Oehlschlaeger, M. A. Shock tube and chemical kinetic modeling study of the oxidation of 2,5-dimethylfuran. *J. Phys. Chem. A* **2013**, *117*, 1371−1392.
(37) Qi, F.; Yang, R.; Yang, B.; Huang, C.; Wei, L.; Wang, J.; Sheng, L.; Zhang, Y. Isomeric identification of polycyclic aromatic hydrocarbons formed in combustion with tunable vacuum ultraviolet photoionization. *Rev. Sci. Instrum.* **2006**, *77*, 084101.
(38) Cai, J.; Zhang, L.; Zhang, F.; Wang, Z.; Cheng, Z.; Yuan, W.; Qi, F. Experimental and Kinetic Modeling Study of n-Butanol Pyrolysis and Combustion. *Energy Fuels* **2012**, *26*, 5550−5568.
(39) Wang, Z.; Cheng, Z.; Yuan, W.; Cai, J.; Zhang, L.; Zhang, F.; Qi, F.; Wang, J. An experimental and kinetic modeling study of cyclohexane pyrolysis at low pressure. *Combust. Flame* **2012**, *159*, 2243−2253.
(40) Zhang, Y.; Cai, J.; Zhao, L.; Yang, J.; Jin, H.; Cheng, Z.; Li, Y.; Zhang, L.; Qi, F. An experimental and kinetic modeling study of three butene isomers pyrolysis at low pressure. *Combust. Flame* **2012**, *159*, 905−917.
(41) Wang, Z.; Ye, L.; Yuan, W.; Zhang, L.; Wang, Y.; Cheng, Z.; Zhang, F.; Qi, F. Experimental and kinetic modeling study on methylcyclohexane pyrolysis and combustion. *Combust. Flame* **2014**, *161*, 84−100.
(42) National Synchrotron Radiation Laboratory. *Photonionization Cross Section Database*, version 1.0; National Synchrotron Radiation Laboratory: Hefei, China, 2011. http://flame.nsrl.ustc.edu.cn/en/database.htm.
(43) Frisch, M. J.; Trucks, G. W.; Schlegel, H. B.; Scuseria, G. E.; Robb, M. A.; Cheeseman, J. R.; Scalmani, G.; Barone, V.; Mennucci, B.; Petersson, G. A., *Gaussian 09*, Revision D.01; Gaussian Inc., 2009.
(44) Design, R.. *CHEMKIN-PRO 15092*; Reaction Design: San Diego, CA, 2009.
(45) Sarathy, S. M.; Vranckx, S.; Yasunaga, K.; Mehl, M.; Oßwald, P.; Metcalfe, W. K.; Westbrook, C. K.; Pitz, W. J.; Kohse-Höinghaus, K.; Fernandes, R. X.; Curran, H. J. A comprehensive chemical kinetic combustion model for the four butanol isomers. *Combust. Flame* **2012**, *159*, 2028−2055.
(46) Tran, L.-S.; Wang, Z.; Carstensen, H.-H.; Hemken, C.; Battin-Leclerc, F.; Kohse-Höinghaus, K. Comparative experimental and modeling study of the low- to moderate-temperature oxidation chemistry of 2,5-dimethylfuran, 2-methylfuran, and furan. *Combust. Flame* **2017**, *181*, 251−269.

DOI: 10.1021/acs.energyfuels.9b00367
Energy Fuels 2019, 33, 4611−4620

(47) Muller, C.; Michel, V.; Scacchi, G.; Côme, G. THERGAS: a computer program for the evaluation of thermochemical data of molecules and free radicals in the gas phase. *J. Chem. Phys.* **1995**, *92*, 1154−1178.
(48) Dooley, S.; Burke, M. P.; Chaos, M.; Stein, Y.; Dryer, F. L.; Zhukov, V. P.; Finch, O.; Simmie, J. M.; Curran, H. J. Methyl Formate Oxidation: Speciation Data, Laminar Burning Velocities, Ignition Delay Times, and a Validated Chemical Kinetic Model. *Int. J. Chem. Kinet.* **2010**, *42*, 527−549.
(49) Dooley, S.; Dryer, F. L.; Yang, B.; Wang, J.; Cool, T. A.; Kasper, T.; Hansen, N. An experimental and kinetic modeling study of methyl formate low-pressure flames. *Combust. Flame* **2011**, *158*, 732−741.
(50) Fisher, E. M.; Pitz, W. J.; Curran, H. J.; Westbrook, C. K. Detailed chemical kinetic mechanisms for combustion of oxygenated fuels. *Proc. Combust. Inst.* **2000**, *28*, 1579−1586.
(51) Rembaum, A.; Szwarc, M. Kinetics of the thermal decomposition of diacetyl peroxide. I. Gaseous phase. *J. Am. Chem. Soc.* **1954**, *76*, 5975−5978.
(52) Glaude, P. A.; Pitz, W. J.; Thomson, M. J. Chemical kinetic modeling of dimethyl carbonate in an opposed-flow diffusion flame. *Proc. Combust. Inst.* **2005**, *30*, 1111−1118.
(53) Bennadji, H.; Coniglio, L.; Billaud, F.; Bounaceur, R.; Warth, V.; Glaude, P.-A.; Battin-Leclerc, F. Oxidation of small unsaturated methyl and ethyl esters. *Int. J. Chem. Kinet.* **2011**, *43*, 204−218.
(54) Fringuelli, F.; Marino, G.; Taticchi, A.; Distefano, F. P.; Pignataro, S. Photoelectron spectra of the α-substituted derivatives of furan, thiophen, selenophen, and tellurophen. A comparative study of the molecular orbital energies. *J. Chem. Soc., Perkin Trans. 2* **1976**, 276−279.
(55) Watanabe, K.; Matsunaga, F. M.; Sakai, H. Absorption Coefficient and Photoionization Yield of NO in the Region 580−1350 Å. *Appl. Opt.* **1967**, *6*, 391−396.
(56) Cool, T. A.; McIlroy, A.; Qi, F.; Westmoreland, P. R.; Poisson, L.; Peterka, D. S.; Ahmed, M. Photoionization mass spectrometer for studies of flame chemistry with a synchrotron light source. *Rev. Sci. Instrum.* **2005**, *76*, 094102.
(57) Yang, B.; Li, Y.; Wei, L.; Huang, C.; Wang, J.; Tian, Z.; Yang, R.; Sheng, L.; Zhang, Y.; Qi, F. An experimental study of the premixed benzene/oxygen/argon flame with tunable synchrotron photoionization. *Proc. Combust. Inst.* **2007**, *31*, 555−563.
(58) Yang, B.; Oswald, P.; Li, Y.; Wang, J.; Wei, L.; Tian, Z.; Qi, F.; Kohsehoinghaus, K. Identification of combustion intermediates in isomeric fuel-rich premixed butanol−oxygen flames at low pressure. *Combust. Flame* **2007**, *148*, 198−209.
(59) Ren, W.; Lam, K.-Y.; Davidson, D. F.; Hanson, R. K.; Yang, X. Pyrolysis and oxidation of methyl acetate in a shock tube: A multi-species time-history study. *Proc. Combust. Inst.* **2017**, *36*, 255−264.

DOI: 10.1021/acs.energyfuels.9b00367
Energy Fuels 2019, 33, 4611−4620